Nanoscale Horizons

ROYAL SOCIETY OF CHEMISTRY

COMMUNICATION

View Article Online
View Journal

Cite this: DOI: 10.1039/d5nh00323g

Received 9th May 2025,
Accepted 8th September 2025

DOI: 10.1039/d5nh00323g

rsc.li/nanoscale-horizons

Unambiguous calibration of power dependence in ratiometric luminescent nanothermometry through multiple intensity ratios and symbolic regression

Simon Spelthann, †*[ab] Lea Koetters,[a] Rajesh Komban, [c] Christoph Gimmler [c] and Michael Steinke [abd]

Ratiometric luminescence nanothermometry carries the potential to measure temperature in situations for which established methods are unsuitable. The precision of nanothermometry depends on the excitation power, so calibration and monitoring of the optical power is mandatory—a requirement that complicates optical setups and limits nanothermometry in scenarios where precise power control or measurement is impractical or unfeasible. Here, we use Er^{3+}-activated nanothermometers and, besides the well-known 525/545 nm ratio, define a second luminescence intensity ratio involving the emission at 660 nm to achieve a power-calibration-free nanothermometry. The intensity of this emission is strongly correlated with the power and is available anyways when using standard spectroscopic instrumentation. We apply symbolic regression to find an unambiguous mathematical expression that describes the experimental data. From this mathematical expression, we determine the mean temperature deviation resulting from the fitting error to be 0.16 K and a maximum temperature precision as small as 6 mK (0.22 K on average). In summary, our approach makes excitation power measurements in ratiometric luminescent nanothermometry superfluous.

New concepts

We demonstrate how optical power calibration in ratiometric nanothermometry can be made superfluous. Ratiometric nanothermometers such as the prominent $NaYF_4$:Er,Yb allow to measure temperature optically and remotely at the nanoscale by comparing the luminescence intensity ratio of two thermally coupled energy levels in lanthanide ions – but only if properly calibrated. If the calibration is not carried out carefully, readout errors of several 100 K can occur. Therefore, every conceivable effect must be considered in addition to the temperature dependence of the emission. This also includes the dependence of the emission on the optical excitation power. Here we found that, by considering a third emission line strongly correlated with the excitation power, we can unambiguously assign the correct temperature to the measured luminescence intensity ratios for different excitation power levels without even knowing the actual power. For this purpose, we applied a machine learning algorithm, namely symbolic regression, to directly fit the power dependency without any optical power measurement. This drastically simplifies the calibration of nanothermometers and, in particular, enables nanothermometry in locations where optical power measurement is not possible, such as highly integrated devices or biological *in vivo* samples.

Temperature is the most fundamental thermodynamic state variable and as such one of the few quantities that play a critical role in nearly all physical, chemical, and biological phenomena.[1–5] The progressive evolution of science and technology to the nanoscale demands increasingly precise temperature measurements on this length scale.[6] To meet this demand, lanthanide-activated nanocrystals have emerged as auspicious tools for ratiometric luminescent nanothermometry. Such nanothermometers, in particular the working horse $NaYF_4$:Er^{3+},Yb^{3+} nanoparticles, allow for temperature monitoring by comparing emission intensities from two thermally coupled 4f transitions within the lanthanide ions.[7] They offer some unique advantages such as well-controllable synthesis or an application temperature spanning from 80 to 900 K.[8]

As the field of nanothermometry grows and matures, the community expands its research focus from material development to physical limitations when performing nanothermometry in real-life applications. Van Swieten and co-workers investigated the impact of noise and background on nanothermometric measurement uncertainties.[9] Vonk *et al.* found that photonic artifacts can result in temperature read-out errors of up to 250 K.[10] Furthermore, lanthanide excitation dynamics involves various nonlinear processes such as excited state

[a] *Leibniz University Hannover, Institute of Quantum Optics, Welfengarten 1, Hannover, Germany. E-mail: spelthann@iqo.uni-hannover.de*
[b] *Cluster of Excellence PhoenixD, Welfengarten 1, Hannover, Germany*
[c] *Fraunhofer Institute for Applied Polymer Research, Center for Applied Nanotechnology, Grindelallee 117, Hamburg, Germany*
[d] *Leibniz University Hannover, QUEST-Leibniz-Research School, Callinstraße 36, Hannover, Germany*
† Present address: Ruhr-University Bochum, Simply Complex Lab, Universitätsstraße 150, Bochum, Germany. E-mail: simon.spelthann@rub.de.

absorption or energy transfer upconversion that introduce an excitation power dependence in nanothermometry.[11] Pickel and co-workers tackled this dependence with rate-equation modeling, which is a complex endeavor.[12–14] Recently, Jia and co-workers found that the dependence of excitation-power in lanthanide-based ratiometric nanothermometers is insensitive to temperature changes and, therefore, can be calibrated.[15]

However, proper calibration of power dependence in nanothermometry is only possible if one can measure the optical power that reaches the lanthanide ions at the application site. This is rarely the case in real-life applications such as biomedical *in vivo* applications[16,17] or highly integrated devices, *e.g.* batteries, that involve optical fibers for excitation power delivery to the nanothermometers.[17–19] Even if measuring the power is possible, it is highly undesirable because additional measurement periphery impairs the optical setups.

Here, we introduce an approach that makes additional optical power measurements superfluous. We used the popular $NaYF_4$:Er^{3+},Yb^{3+} as a model nanothermometer on the tip of an optical fiber using the common ratio between the Erbium-emission at 525 nm ($^2H_{11/2}$ level) and 545 nm ($^4S_{3/2}$ level). Instead of measuring the optical power at the tip of the fiber - which is an impossible endeavor if the fiber is employed as an endoscopic sensor - we consider a second luminescence intensity ratio that involves a third emission line at 660 nm originating from the $^4F_{9/2}$ level. This emission is strongly excitation power-dependent and its spectroscopic information available anyway. We apply a machine learning algorithm, specifically, symbolic regression, to fit an analytical expression to the experimental data. The resulting expression allows us to determine the temperature of the nanothermometers without knowing the optical power delivered through the fiber with a mean precision of 0.22 K. Our approach can be applied to any material that provides a predominantly power-dependent third emission. Our work showcases how to unambiguously calibrate the power dependency in ratiometric luminescent nanothermometers only through spectroscopic information. Hence, power dependence is no longer a challenges in nanothermometry.

Nanocrystals activated with Erbium ions are the most prominent and, strikingly, also the most versatile nanothermometers.[20] We synthesized ellipsoidal β-$NaYF_4$:Er^{3+},Yb^{3+}@$NaYF_4$ core@shell nanocrystals ((16.3 ± 0.5) nm × (26.8 ± 0.55) nm, *c.f.* Fig. 1a and b) that predominantly emit green luminescence under infrared excitation at 980 nm (Fig. 1c) and attached them to an optical multimode

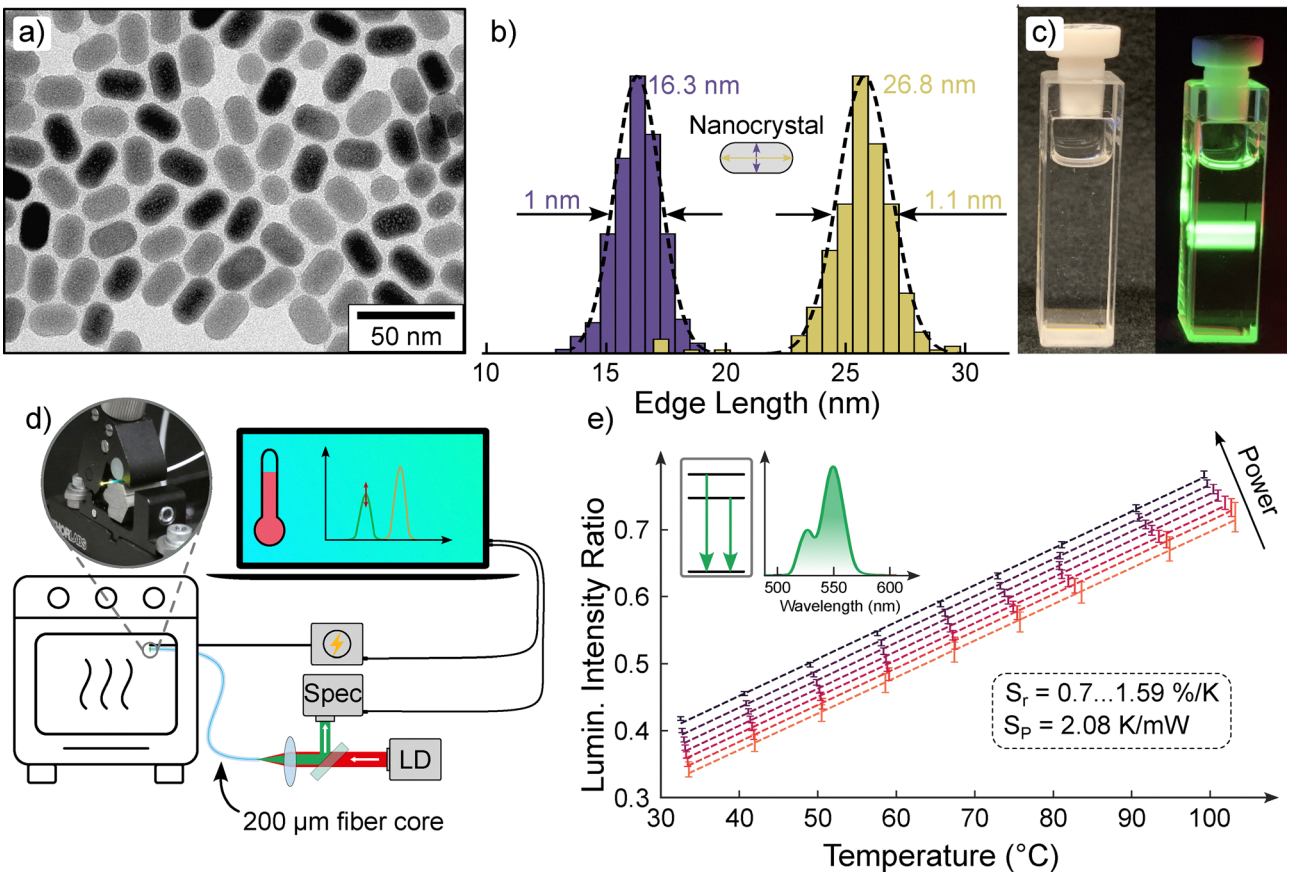

Fig. 1 (a) Transmission electron microscope image of the as-prepared core@shell nanocrystals and (b) the corresponding size distributions of their two axes. (c) Photograph of the predominantly green emission occuring under laser excitation at 980 nm. (d) The fiber sensor tip is placed in an furnace together with an electrical sensor that serves for calibration. The spectrometer for read-out and the electric sensor are connected to a computer for automated readout. (e) The luminescence intensity ratio of the two emission lines (inset) has a sensitivity of 0.7–1.59% K^{-1} and exhibits a power-dependence with a sensitivity of 2.08 K mW^{-1}.

fiber with a core diameter of 200 μm (see details in the SI). Similar fiber tip sensor concepts were reported before[21] and it allowed us to conveniently perform temperature-dependent spectroscopy experiments with the nanothermometers inside a furnace (*c.f.* Fig. 1d). We characterized the luminescence intensity ratio for different excitation powers during a cool-down period of the furnace from about 100 °C to room temperature (*c.f.* Fig. 1e).

Ratiometric luminescent nanothermometers are typically calibrated *via* the ratio

$$\frac{I(\lambda_1 = 525\,\mathrm{nm})}{I(\lambda_2 = 545\,\mathrm{nm})} \equiv R = A \cdot \exp\left(\frac{-\Delta E}{k_B T}\right), \qquad (1)$$

where $I(\lambda)$ represents the spectrally-integrated intensities at the respective wavelengths, ΔE is the energy gap between the $^2H_{11/2}$ and $^4S_{3/2}$ level (theoretically in the range of 87–100 meV[22]), k_B is the Boltzmann constant, and A is a constant based on the spontaneous emission rates from $^2H_{11/2}$ and $^4S_{3/2}$ to $^4I_{15/2}$. Since we used Erbium-activated nanothermometers in comparatively small temperature ranges, we approximated the exponential relationship in eqn (1) with a linear fit. Fig. 1e depicts the luminescence intensity ratio with the linear fits. We calculated the relative sensitivity,

$$S_r(T) = \frac{1}{R(T)}\left|\frac{\Delta R}{\Delta T}\right|, \qquad (2)$$

of the thermometer to vary between S_r = 0.7–1.59% K^{-1}. We achieve high relative sensitivity of 1.59% K^{-1} for low temperatures around 30 °C for optical powers of around 3 mW in the fiber. For powers as high as 10 mW, the relative sensitivity decreases to 1.32% K^{-1} at around 30 °C. At high temperatures around 100 °C, the relative sensitivity decreases to values between 0.76% K^{-1} (10 mW) and 0.79% K^{-1} (3 mW). These relative sensitivities correspond to the typical values reported for Erbium-activated nanothermometers. Increasing the excitation power produces an offset to the luminescence intensity ratio resulting in a systematic measurement error of up to 2.08 K mW^{-1} (compared to up to 0.42 K mW^{-1} in the work by Pickel *et al.*[12]).

Here, we make use of the fact that nonlinear effects such as energy transfer upconversion or excited state absorption that result in occupation of the green-emitting energy levels also lead to efficient occupation of the red-emitting energy level at high excitation energies. At low excitation powers, the number of infrared photons is only sufficient to excite the green

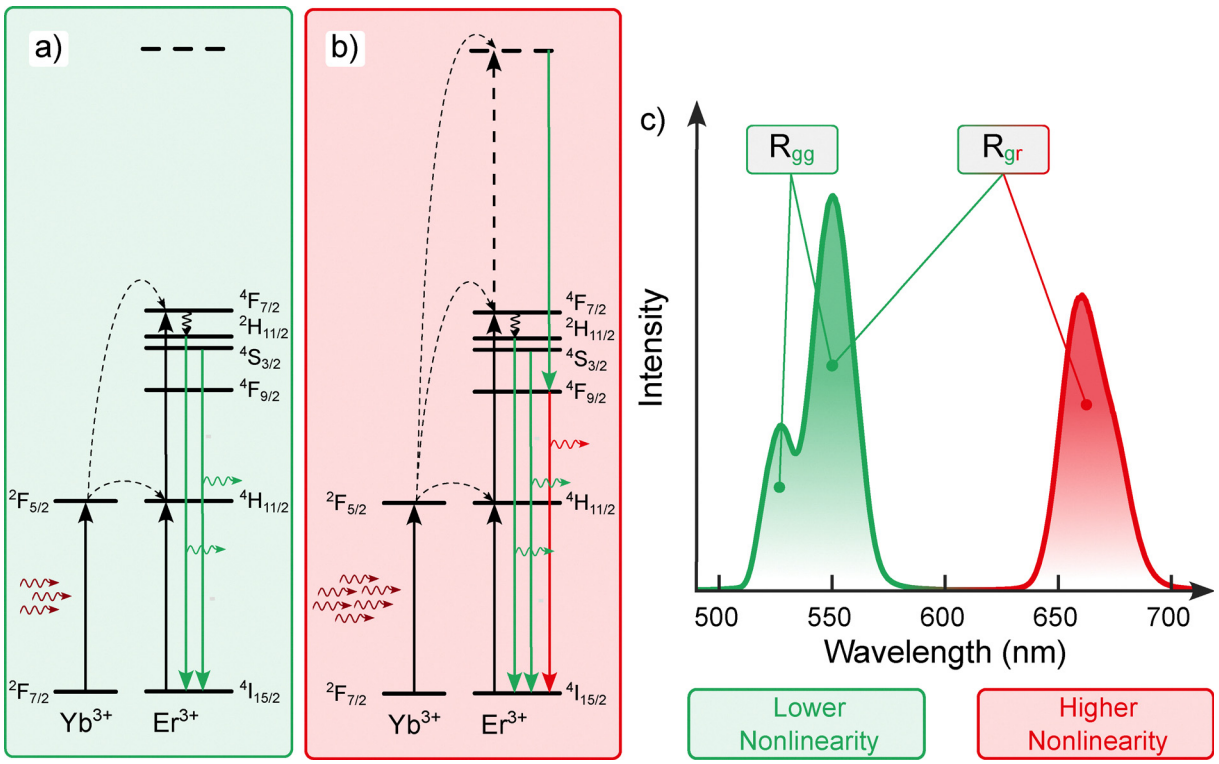

Fig. 2 The excitation mechanisms for the green and red emission strongly differ: (a) the green emission results mainly from the absorption of two infrared photons by Ytterbium ions whose excitation energy is transferred to Erbium ions (energy transfer upconversion, ETU). ETU is highly nonlinear. The intensity ratio of the resulting green emissions is temperature dependent due to their thermal coupling as described by Boltzmann's law. (b) At higher optical powers, the two-for-one-process described in (a) extends to a three-for-two-process involving three absorbed infrared photons and one green and one red photon (the upper dashed line indicates a manifold of higher energy levels, see SI for details). The nonlinearity of this process is even higher than for classical ETU and can be exploited for power calibration. (c) Defining a second luminescence intensity ratio involving the red emission allows for unambiguous calibration of nanothermometers.

emissions (approximately two infrared photons generate one green photon). The ratio of the dominant green emissions is predominantly temperature-dependent (*c.f.* Fig. 2a). At high excitation powers, the nonlinearity is strong enough to even excite higher energy levels that first relax by emitting one photon in the green spectral range and as such slightly influence the luminescence intensity ratio as defined in eqn (1). The final energy level of this green transition is the red-emitting level that is efficiently occupied by this mechanism and as a result emits a second, red photon (*c.f.* Fig. 2b). As a consequence, this emission is predominantly excitation power-dependent (approximately three infrared photons generate one green photon and one red photon, *c.f.* Fig. S4).

We exploit the different excitation pathways of the green and red emissions to unambiguously calibrate the nanothermometers.[23] For that, we define a first luminescence intensity ratio as the ratio between the intensities at 525 nm and 545 nm (R_{gg}) and a second ratio between the intensities at 545 nm and 660 nm (R_{gr}, *c.f.* Fig. 2c). To analyze the data, we applied a machine learning algorithm. Recently, machine learning approaches have been successfully employed to analyze nanothermometry data, *e.g.* multiparameter regression.[24,25] Here, we employ symbolic regression for the first time which is an established machine learning approach based on evolutionary computation for searching mathematical expressions while minimizing various error metrics. In contrast to other machine learning approaches, symbolic regression yields an interpretable result and allows researchers to find natural laws from experimental data.[26–28]

Fig. 3a shows the cross-validation we performed for an increasing dataset size to verify that our maximum dataset size

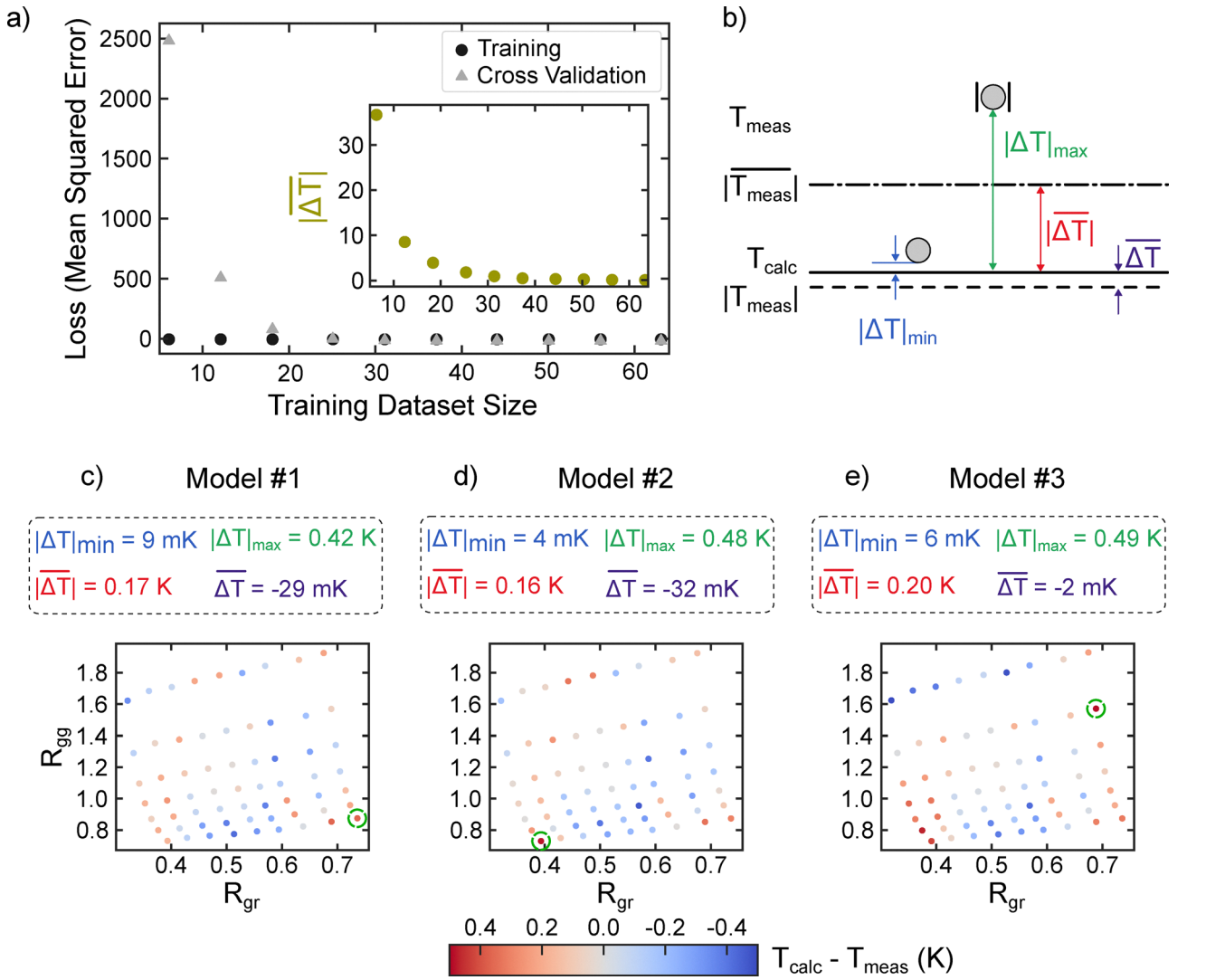

Fig. 3 (a) With an increasing dataset size, the loss (mean squared error) of the cross validation data subset converges to that of the training dataset, which coincides with a decrease of the mean absolute temperature difference between model and experiment (inset). (b) Different error metrics defined to determine the quality of a model: maximum ΔT (red), minimum absolute ΔT (blue), maximum absolute ΔT (green, employed error metric in the model optimization), minimum ΔT (purple), mean absolute ΔT (yellow), mean ΔT (orange). (c)–(e) Three best models, their error metrics, and color-coded deviation from the measurement. The green circle marks the position of the maximum absolute error.

is sufficiently large. The loss, *i.e.* the mean squared error is very high for small dataset sizes because the amount of data is insufficient for high quality regression. It converges at larger dataset sizes which corresponds to a decrease of the mean temperature difference $\overline{\Delta T}$ to ≈ 0.5 K (*c.f.* inset in Fig. 3a).

We tuned the hyperparameters of the modelling *via* Bayesian optimization by minimizing $|\Delta T_{\max}|$ (*c.f.* Fig. 3b and SI for details on the optimization) and fitted the model to our data. The difference between the temperature calculated from the fitted model T_{calc} and the measured temperature T_{meas} is depicted in Fig. 3c to e for the models obtained from the three best hyperparameters. The resulting mathematical expressions significantly differ for each model which is why the position of the maximum absolute error $|\Delta T_{\max}|$ (green circle in Fig. 3) varies for each model. However, its value changes only in the second decimal. From the physical plausibility of the respective mathematical expressions, we decided to continue with the first model whose expression reads:

$$T(R_{\text{gg}}, R_{\text{gr}}) = -0.111692 - \frac{5.80994}{R_{\text{gg}}} + 1.06419 \cdot R_{\text{gr}} \cdot R_{\text{gg}} \cdot (147.42 + R_{\text{gg}}) - \frac{5.02848}{R_{\text{gr}}^{3.11032}}. \quad (3)$$

Note that this expression is not so much a correct description of the physics involved but the equation that is found by the symbolic regression to deviate the least from the measured data. While the model yielded by the symbolic regression allows for accurate interpolation within the constrained parameter space it certainly lacks accuracy towards extrapolation. Yet, eqn (3) strikingly includes power-law expressions for R_{gr} which is in accordance with Jia *et al.*.[15] Eventually, the found expression allows us to determine the temperature for given R_{gg} and R_{gr}. Furthermore, we can calculate the sensor's sensitivity analytically which is possible through the interpretable result obtained from the symbolic regression. The relative sensitivity of nanothermometers is given by the inverse partial derivative normalized to the luminescence intensity ratio (*c.f.* eqn (2)). Thus, we can calculate said sensitivity from the root mean square of eqn (3)'s gradient vector field. Using this sensitivity, our approach allows us to analytically calculate the absolute temperature precision *via*

$$\delta T = \pm \frac{1}{S_{\text{r}}} \left| \frac{\Delta R}{R} \right|. \quad (4)$$

The relative sensitivity and temperature precision is depicted in Fig. 4. We show the temperature and optical power in the fiber alongside the luminescence intensity ratios to demonstrate that the latter are coupled to real physical quantities. However, measuring these quantities is not necessary to determine the characteristic properties of the nanothermometer. Instead, knowledge of the luminescence intensity ratios is sufficient.

Both metrics have their maximum at high powers and low temperatures because the respective single sensitivities are highest for high powers and low temperatures (*c.f.* Fig. 1e). Since the calculated sensitivity is a root mean square of both, the temperature and power sensitivity, it is is high compared to typical values reported for nanothermometers.[29]

The temperature precision is about 6 mK at maximum which is very good and a result of the high sensitivity. However, the total temperature deviation is

$$\delta T_{\text{total}} = T_{\text{calc}} - T_{\text{meas}} + \delta T \quad (5)$$

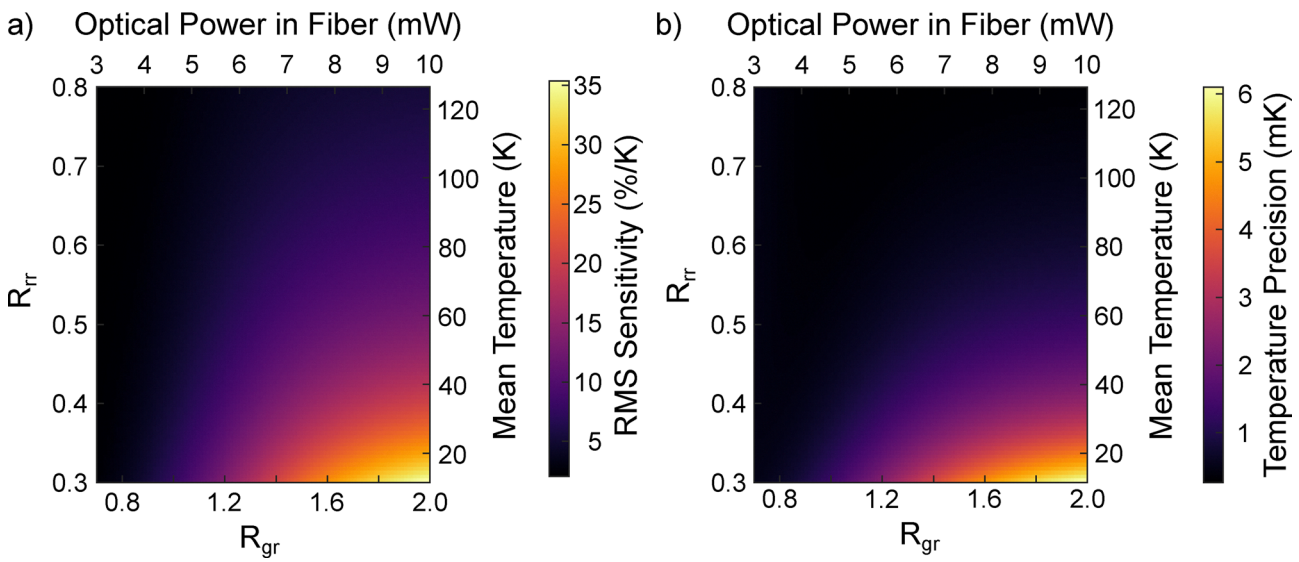

Fig. 4 (a) The root mean square of the individual relative sensitivity gradient vector field yields the mean sensitivity of the nanothermometers. The sensitivity is best for low temperatures and medium optical powers. While the first is expected from the literature, the second is unexpected and cannot be explained by employing symbolic regression. More complex numerical modeling or experiments are necessary to understand the physics of this behaviour. (b) The relative sensitivity yields the absolute temperature precision of the nanothermometers. The maximum temperature precision is 6 mK for high optical powers and low temperatures. For high temperatures and low optical powers, the temperature precision is below 1 mK.

which results in a mean temperature precision of 0.22 K and a worst-case temperature precision of 0.54 K.

In summary, we attached β-$NaYF_4$:Er^{3+},Yb^{3+} nanocrystals on a fiber facet and used their temperature-dependent luminescence to measure temperature. By defining a second luminescence intensity ratio that includes the red emission at 660 nm we introduced a measurable quantity that is strongly correlated with the optical excitation power. We employed a symbolic regression algorithm to yield an analytical expression that describes the temperature for the two different intensity ratios. Our approach exhibits a maximum relative root mean square sensitivity of 35% K^{-1} and a mean temperature precision of 0.22 K. It allows unambiguous calibration of the power dependency in Erbium-activated ratiometric luminescent nanothermometers and can be extended to any activator such as Tm^{3+} or Ho^{3+} as long as it provides predominantly power-dependent optical transitions. Furthermore, the approach enables direct analytical determination of a nanothermometer's characteristic properties such as its sensitivity. With our approach, the excitation power of ratiometric luminescent nanothermometers no longer needs to be measured, which drastically simplifies their calibration and respective optical setups. Towards applications, this is a huge benefit, in particular in minimally-invasive scenarios such as *in vivo* applications.

Author contributions

Conceptualization: S. S. and M. S., data curation: S. S. and M. S., formal analysis: S. S. and M. S., funding acquisiton: N/A, investigation: S. S., L. K., R. K., M. S., methodology: S. S. and M. S., project administration: S. S., C. G., M. S., resources: S. S., C. G., M. S., software: S. S., supervision: S. S., C. G., M. S., validation: S. S. and M. S., visualization: S. S., writing – original draft: S. S., writing – review & editing: all.

Conflicts of interest

There are no conflicts to declare.

Data availability

The data supporting this article have been included as part of the SI. The raw spectra are available at Zenodo under DOI: **https://doi.org/10.5281/zenodo.16918385**. Supplementary information: particle synthesis, structural characterization, sensor fabrication, optical experiments and characterization, hyperparameter optimization, and cross-validation. See DOI: **https://doi.org/10.1039/d5nh00323g**.

Acknowledgements

The authors thank Birgit Stiller for her support. Partly funded by the Deutsche Forschungsgemeinschaft (DFG, German Research Foundation) under Germany's Excellence Strategy – EXC-2123 QuantumFrontiers – 390837967. L. K. acknowledges funding by the Deutsche Forschungsgemeinschaft (DFG, German Research Foundation) under Germany's Excellence Strategy within the Cluster of Excellence PhoenixD (EXC 2122, Project ID 390833453).

References

1 P. R. N. Childs, J. R. Greenwood and C. A. Long, *Rev. Sci. Instrum.*, 2000, **71**, 2959–2978.
2 J. Nicholas and D. White, *Traceable Temperatures: an introduction to temperature measurement and calibration*, Wiley, 1994, vol. 8.
3 P. R. Childs, *Pratical Temperature Measurement*, Butterworth-Heinemann, 2001.
4 L. Michalsi, K. Eckersdorf, J. Kucharski and J. McGhee, *Temperature Measurement*, John Wiley Sons Ltd., 2002.
5 M. R. Moldover, W. L. Tew and H. W. Yoon, *Nat. Phys.*, 2016, **12**.
6 C. D. S. Brites, R. Marin, M. Suta, A. N. Carneiro Neto, E. Ximendes, D. Jaque and L. D. Carlos, *Adv. Mater.*, 2023, **35**, 2302749.
7 F. Vetrone, R. Naccache, A. Zamarrón, A. Juarranz de la Fuente, F. Sanz-Rodríguez, L. Martinez Maestro, E. Martín Rodriguez, D. Jaque, J. García Solé and J. A. Capobianco, *ACS Nano*, 2010, **4**, 3254–3258.
8 M. Suta, *What makes β-NaYF4:Er^{3+},Yb^{3+} such a successful luminescent thermometer?*, Royal Society of Chemistry, 2025, vol. 17.
9 T. P. van Swieten, A. Meijerink and F. T. Rabouw, *ACS Photonics*, 2022, **9**, 1366–1374.
10 S. J. W. Vonk, T. P. van Swieten, A. Cocina and F. T. Rabouw, *Nano Lett.*, 2023, **23**, 6560–6566.
11 J. Zhou, B. del Rosal, D. Jaque, S. Uchiyama and D. Jin, *Nat. Methods*, 2020, **17**, 967–980.
12 A. D. Pickel, A. Teitelboim, E. M. Chan, N. J. Borys, P. J. Schuck and C. Dames, *Nat. Commun.*, 2018, 9.
13 P. Villanueva-Delgado, K. W. Krämer, R. Valiente, M. de Jong and A. Meijerink, *Phys. Chem. Chem. Phys.*, 2016, **18**, 27396–27404.
14 F. Pini, L. Francés-Soriano, N. Peruffo, A. Barbon, N. Hildebrandt and M. M. Natile, *ACS Appl. Mater. Interfaces*, 2022, **14**, 11883–11894.
15 M. Jia, M. Li, D. Li, X. Zhang and G. Chen, *Nano Lett.*, 2024, **24**, 15450–15456.
16 B. Zhou, K. Fan, J. Zhai, C. Jin and L. Kong, *Adv. Sci.*, 2023, **10**, 2303527.
17 I. V. Fedotov, M. A. Solotenkov, M. S. Pochechuev, O. I. Ivashkina, S. Y. Kilin, K. V. Anokhin and A. M. Zheltikov, *ACS Photonics*, 2020, **7**, 3353–3360.
18 H. Zhang, J. Ye, X. Wang, S. Zhao, R. Lei, L. Huang and S. Xu, *J. Mater. Chem. C*, 2019, **7**, 15269–15275.
19 H. Li, F. Wei, Y. Li, M. Yu, Y. Zhang, L. Liu and Z. Liu, *J. Mater. Chem. C*, 2021, **9**, 14757–14765.
20 M. Suta and A. Meijerink, *Adv. Theory Simul.*, 2020, **3**, 2000176.
21 R. S. Baltieri, A. Reupert, D. Manzani and L. Wondraczek, *Adv. Mater. Technol.*, 2025, **10**, 2401877.
22 S. Zhou, K. Deng, X. Wei, G. Jiang, C. Duan, Y. Chen and M. Yin, *Opt. Commun.*, 2013, **291**, 138–142.

23 M. Kraft, C. Wuerth, V. Muhr, T. Hirsch and U. Resch-Genger, *Nano Res.*, 2018, **11**, 6360–6374.
24 F. E. Maturi, C. D. S. Brites, E. C. Ximendes, C. Mills, B. Olsen, D. Jaque, S. J. L. Ribeiro and L. D. Carlos, *Laser Photonics Rev.*, 2021, 15.
25 D. G. Stone, Y. Chen, E. A. Ekimov, T. T. Tran and C. Bradac, *ACS Appl. Opt. Mater.*, 2023, **1**, 898–905.
26 M. Schmidt and H. Lipson, *Science*, 2009, **324**, 81–85.
27 Z. Li, J. Ji and Y. Zhang, *arXiv*, preprint, arXiv.2111.12210, 2021, DOI: **10.48550/arXiv.2111.12210**.
28 P. Lemos, N. Jeffrey, M. Cranmer, S. Ho and P. Battaglia, *Mach. Learn. Sci. Technol.*, 2023, **4**, 045002.
29 L. Marciniak, K. Prorok and A. Bednarkiewicz, *J. Mater. Chem. C*, 2017, **5**, 7890–7897.